Noninvasive and Accurate Measuring Method of the MMC and HVDC Circuit Breaker Action Moment Based on Transient E-Field Pulse

Xu Kong, Yan-zhao Xie, *Senior Member, IEEE*, Wen-qi Xing, Zhen-dong Sun, *Senior Member, IEEE*, Shao-yin He, *Member, IEEE*, Li Liu, Peng Qiu, Xiao-jun Ni, and Kun Zhang

***Abstract*— This article introduces the measurement and analysis of the transient electric field (E-field) derived from the switching operation of the modular multilevel converter (MMC) and the high voltage direct current (HVdc) circuit breaker (CB) in a 200 kV converter station constructed in the Zhoushan Islands, China. It is revealed that the switching transient E-field in the converter station is a quasi-static field. Although the switching E-field pulse is a kind of electromagnetic interference to the secondary electronic circuit of the converter station, it can be used to accurately monitor the action moment of the MMC and the CB. The action moment of the MMC and the CB can be measured with an error of less than 0.005 ms based on the steep pulse front of the switching E-field pulse. This result, which is far more accurate compared to the measurement using the voltage recording system that comes with the converter station. This is of significance to the relay protection of the HVdc transmission system whose fault rapidly develops. Additionally, this method has the advantage of being noninvasive, flexible, and low cost. It has potential application value in the condition monitoring of the MMC and the HVdc CB.**

***Index Terms*—Condition monitoring, electric field, hybrid high voltage direct current (HVdc) circuit breaker, HVdc transmission, modular multilevel converter (MMC).**

I. Introduction

MODULAR multilevel converter (MMC) based high voltage direct current (HVdc) transmission has attracted widespread attention from industry and academia in recent years [1], [2]. It is of great significance to submarine cable transmission, renewable energy integration, and grid interconnection. Compared with the ac transmission system, the HVdc transmission system has lower damping. Therefore, its faults develop faster, and correspondingly, its protection is more difficult. For instance, the short-circuit current can reach its maximum value in just a few milliseconds when a short-circuit fault occurs on a dc line. This is much faster than the rise of the ac line fault current. Since the blocking of the MMC cannot completely break the short-circuit current due to the freewheel diode, it is also necessary to disconnect the ac circuit breaker (CB) of the MMC. However, it takes a dozen or even dozens of milliseconds to disconnect the ac CB. This is detrimental to the safety of the electric power equipment. Therefore, the HVdc CB is required to quickly interrupt the short-circuit current and dissipate the large amount of energy stored in the system inductance.

The condition monitoring of the MMC and the HVdc CB is essential to ensure the safe operation of the dc grid. The action time sequence and action moment of the MMC and the HVdc CB should be accurately recorded to evaluate their relay protection performance when a fault occurs. However, the fault recording system that comes with the converter station usually has a limited measurement bandwidth. In engineering practice, its digital sampling rate generally does not exceed 10 ksps. Hence, the measurement error of the relay protection action moment of the MMC and HVdc CB is not less than 0.1 ms. The measurement error on this time scale may be negligible for the ac system. However, it needs to be considered for the dc system whose fault develops faster. Therefore, it is necessary to improve the measurement accuracy of the action moment to evaluate the jitter and reliability of the relay protection operation of MMC and HVdc CB. In addition, improving the measurement accuracy of the moment when the short-circuit fault occurs can improve the accuracy of fault location, thus making the maintenance of the submarine cable more convenient.

The switching of the operating mode of the MMC and the operation of the CB will cause a strong transient electromagnetic field in the converter station. For the low-voltage communication and control circuit of the converter station, it is a kind of radiated electromagnetic interference (EMI). Therefore, many researchers have studied the switching transient electromagnetic

Manuscript received 9 February 2022; revised 9 May 2022; accepted 22 June 2022. Date of publication 27 June 2022; date of current version 26 July 2022. This work was supported by Shandong Natural Science Foundation under Grant ZR2020ZD26. Recommended for publication by Associate Editor B. Singh. *(Corresponding author: Xu Kong.)*

Xu Kong and Zhen-dong Sun are with the College of Electrical Engineering and Automation, Shandong University of Science and Technology, Tsingtao 266590, China (e-mail: kongxu.nachuan@foxmail.com; zhendong.sun@amss.ac.cn).

Yan-zhao Xie and Shao-yin He are with the State Key Laboratory of Electrical Insulation and Power Equipment, School of Electrical Engineering, Xi'an Jiaotong University, Xi'an 710049, China (e-mail: yzxie@xjtu.edu.cn; shaoyin.he@xjtu.edu.cn).

Wen-qi Xing is with the Pinggao Group Co., Ltd., Pingdingshan 467000, China (e-mail: xingwenqi@126.com).

Li Liu, Peng Qiu, and Xiao-jun Ni are with the State Grid Zhejiang Electric Power Company, Hangzhou 310014, China (e-mail: liulidido@163.com; qiupeng5000@163.com; nixiaojun89@163.com).

Kun Zhang is with the XJ Electric Co., Ltd., Xuchang 461000, China (e-mail: kongnachuan@163.com).

Color versions of one or more figures in this article are available at https://doi.org/10.1109/TPEL.2022.3186484.

Digital Object Identifier 10.1109/TPEL.2022.3186484

(EM) environment in the substation and the converter station. For example, Wiggins *et al.* [3] conducted many measurement experiments in various substations of different types and voltage levels to summarize the characteristics of the switching transient refers to EM environment and validate the developed EMI prediction models. Zhang *et al.* [4], [5] investigated the characteristics of the radiated electric field (E-field) in the MMC-HVdc station.

For another perspective, the switching transient EM field contains a wealth of information about the operation status of the MMC and CB, especially the operating moment of the devices. For example, Moore *et al.* [6], [7] verified that the interpole switching times of the three-phase CB can be measured and calculated by the switching E-field. Roldan *et al.* [8] proposed a nonintrusive method to detect the reignition of the CB by measuring the switching E-field pulse. Chapman [9] discussed the possibilities and limitations of the arc duration measurement in HVac CB by the switching transient EM field. In addition, it is possible to detect and locate certain types of partial discharges in substations by measuring the radiated E-field pulse [10]. Moreover, a previous paper has proposed a method of insulation fault diagnosis for CB based on the switching E-field [11].

It can be inferred from previous research results that the relay protection action moment of the MMC and HVdc CB can be accurately measured by the switching E-field pulse. To verify the effectiveness and accuracy of this method, this article measures and analyzes the transient E-field pulse in a 200 kV converter station under the artificial short-circuit test. Section II introduces the overall experiment configuration. In Section III, the mathematical formulae of the linear correspondence between the E-field of the power transmission line and its voltage are derived. In Section IV, the switching E-field pulses of the MMC and HVdc CB are measured and analyzed. Finally, the advantages and limitations of the switching E-field pulse-based MMC and HVdc CB action moment measurement method are summarized in Section V.

II. Overall Experiment Configuration

A. Scheme of the Short-Circuit Test for the MMC and HVDC CB Based Converter Station

A $\pm$200kV five-terminal voltage source converter based HVdc transmission project is constructed in Zhoushan Islands, China, to supply power to the five main islands, as illustrated in Fig. 1. Two hybrid HVdc CBs are installed at the Zhouding converter station to improve the protection capability of the system against dc faults. Because the current interruption ability is the key performance of the CB, artificial short-circuit tests were performed at the Zhouding converter station to check the short-circuit current interruption ability of the HVdc CB [12], [13]. Concurrently, the switching transient EM environment of interest during the artificial short-circuit test was measured.

Fig. 2 presents the schematic diagram of the Zhouding converter station with a rated capacity of 400 MW. Since it has no ground point, it is a pseudobipolar HVdc system. From the perspective of space layout, the converter station has three adjacent halls. The main ac equipment, such as the ac CBs, the current-limiting resistors, and the reactors, are installed in

Fig. 1. Five-terminal HVdc transmission system in the Zhoushan Islands.

Hall 1. The current-limiting resistors are connected in series to the main circuit when the MMC is charged and are bypassed by disconnectors when the MMC works normally. The MMC valve is installed in Hall 2. Typically, the MMC operates in the nearest level modulation (NLM) mode. Each valve arm has 270 half-bridge submodules, of which 250 and 20 are in working state and standby state, respectively. The inside of the valve hall is exhibited in Fig. 3. Two 200 kV hybrid HVdc CBs are installed in Hall 3. Smoothing reactors are inserted between the CBs and the dc cables to suppress the rising rate of the fault current. The distance between the smoothing reactor and the short-circuit point is approximately 140 m.

B. Structure and Working Principle of the Hybrid HVDC CB

Figs. 4 and 5 illustrate the photo and circuit schematic diagram of the 200 kV hybrid HVdc CB, respectively. It is composed of three branches in parallel: branch 1 (the main current branch), branch 2 (the current commutation branch), and branch 3 (the energy dissipation branch). The main current branch is composed of an ultrafast mechanical switch and a power electronic switch in series. The power electronic switch consists of 6 IGBT-based full-bridge submodules (FBSM), 2 in parallel and 3 in series, with a 115μF capacitor in each FBSM. The current commutation branch comprises over one hundred FBSMs in series, and the equivalent capacitance of the entire branch in the blocking state is about 1μF. The energy dissipation branch is a string of metal oxide varistors (MOV).

The basic opening progress of the hybrid HVdc CB is to insert the MOV into the current loop. Under normal operating conditions, the rated current is carried by branch 1. The fault current is first forced to commutate from branch 1 to branch 2 by blocking the FBSMs in branch 1 when a short-circuit fault occurs. Then, the ultrafast mechanical switch is disconnected to guarantee that branch 1 is completely disconnected. The FBSMs in branch 2 are blocked and the capacitors in branch 2 start to charge when the distance between the contactors of the ultrafast mechanical switch is large enough. The voltage across the MOV continues to rise until its breakover voltage, and then the fault

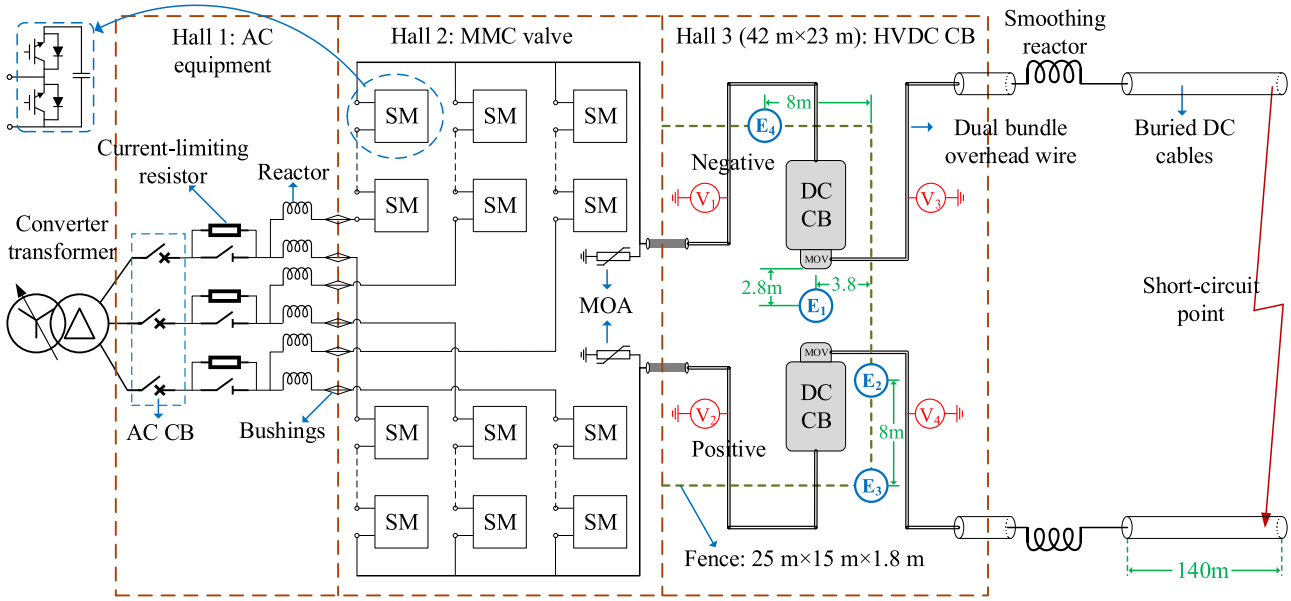

Fig. 2. Schematic diagram of the Zhouding converter station and the distribution map of the E-field pulse measurement points.

Fig. 3. Photo of the MMC in the valve hall.

Fig. 4. Photo of the hybrid HVdc CB in Hall 3.

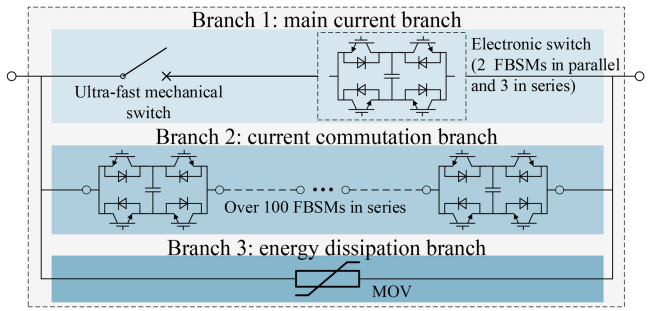

Fig. 5. Circuit schematic diagram of the hybrid HVdc CB.

current commutates to branch 3. Finally, the MOV returns to a high-impedance state after the energy stored in the system inductance is consumed, completing the breaking process of the CB. In addition, as shown in Fig. 2, two metal oxide arresters (MOA) are installed on the positive and negative busbars between the MMC and the CB. Concerning the pseudobipolar HVdc system, the MOAs can not only limit the overvoltage but also dissipate part of the energy stored in the system inductance when the most common single-pole-to-ground short-circuit fault occurs.

C. Measurement Scheme of the Voltage and the Transient E-field Pulse

An electrical small rod antenna and optical fiber transmission-based E-field measurement system is developed to measure the switching transient E-field pulse in substations or converter stations [14]. Its measurement bandwidth ranges from 200 Hz to 680 MHz. As indicated in Fig. 2, four E-field probes are placed next to the two CBs in Hall 3. Probe No. 1 is placed on the ground, in the middle of the two CBs. Probes No. 2 to 4 are placed on the top of the iron fence. The E-field signals measured by the probes

are transmitted through the optical fiber to the oscilloscope in the remote shielded room.

The measurement bandwidth of the original voltage and current monitoring system of the converter station is limited, with the maximum sampling rate of only 10 ksps. Four resistance-capacitance voltage dividers, V_1 to V_4, are installed on both sides of the two CBs to accurately record the transient process during the test, as displayed in Fig. 2. The operating bandwidth of the voltage divider ranges from dc to 1 MHz. The measured voltage signals are recorded by an oscilloscope placed in the shielded room, with a sampling rate of 25 Msps.

III. Verification of the Linear Correspondence Between the E-field of the High-Voltage Equipment and Its Voltage

A. E-field of the High-Voltage Equipment is an Electric Quasi-Static Field

According to the Helmgoltz's theorem, a general E-field $\vec{E}$ can be considered as the sum of an irrotational field $\vec{E}_1$ and a solenoidal field $\vec{E}_2$ [15]. The irrotational field can be considered as the negative gradient of a scalar potential function $\varphi(\vec{r})$ and the solenoidal field can be considered as the curl of a vector potential function $\vec{A}(\vec{r})$, as expressed in (1). The calculation formulas of the two potential functions, $\varphi(\vec{r})$ and $\vec{A}(\vec{r})$, are provided in (2) and (3). $\vec{E}_1$ represents the Coulomb E-field generated by the electric charge on the conductors. $\vec{E}_2$ indicates the induced E-field generated by the time-varying magnetic field

$$\vec{E} = \vec{E}_1 + \vec{E}_2 = -\nabla\varphi(\vec{r}) + \nabla \times \vec{A}(\vec{r}) \tag{1}$$

$$\varphi(\vec{r}) = \frac{1}{4\pi}\int_{\mathrm{V}'} \frac{\nabla' \cdot \vec{E}(\vec{r}')}{|\vec{r}-\vec{r}'|}\mathrm{dV}' - \frac{1}{4\pi}\int_{\mathrm{S}'} \frac{\vec{E}(\vec{r}')\cdot\vec{n}'}{|\vec{r}-\vec{r}'|}\mathrm{dS}' \tag{2}$$

$$\vec{A}(\vec{r}) = \frac{1}{4\pi}\int_{\mathrm{V}'} \frac{\nabla' \times \vec{E}(\vec{r}')}{|\vec{r}-\vec{r}'|}\mathrm{dV}' + \frac{1}{4\pi}\int_{\mathrm{S}'} \frac{\vec{E}(\vec{r}')\times\vec{n}'}{|\vec{r}-\vec{r}'|}\mathrm{dS}'. \tag{3}$$

The space inside the hall is chosen as the volume V' in (3) to investigate the E-field in the hall in Fig. 4. The closed surface consisting of the hall walls, the outer surfaces of the conductors and the ground is chosen as the S' in (3). Since the hall is large, the E-field outside the hall can be considered zero. Hence, the tangential component of the E-field on the closed surface S' is zero, as expressed in

$$\vec{E}(\vec{r}') \times \vec{n}'\Big|_{\mathrm{S}'} = 0. \tag{4}$$

Faraday's law of electromagnetic induction suggests that, the curl of the E-field is equal to the negative derivative of the magnetic field with respect to time

$$\nabla \times \vec{E} = -\frac{\partial \vec{B}}{\partial t}. \tag{5}$$

Substitution of (4) and (5) in (3) yields

$$\begin{aligned}
\vec{E}_2 = \nabla \times \vec{A}(\vec{r}) &= \nabla \times \left[\frac{1}{4\pi}\int_{\mathrm{V}'} \frac{\nabla' \times \vec{E}(\vec{r}')}{|\vec{r}-\vec{r}'|}\mathrm{dV}'\right] \\
&= \frac{1}{4\pi}\nabla \times \int_{\mathrm{V}'} \left[\frac{-\frac{\partial \vec{B}(\vec{r}')}{\partial t}}{|\vec{r}-\vec{r}'|}\partial t\right]\mathrm{dV}' = \frac{1}{4\pi}\int_{\mathrm{V}'} \left[\nabla \times \frac{\frac{\partial \vec{B}(\vec{r}')}{\partial t}}{|\vec{r}-\vec{r}'|}\right]\mathrm{dV}' \\
&= -\frac{1}{4\pi}\int_{\mathrm{V}'} \left[\left(\nabla \frac{1}{|\vec{r}-\vec{r}'|}\right) \times \frac{\partial \vec{B}(\vec{r}')}{\partial t} + \frac{1}{|\vec{r}-\vec{r}'|}\nabla \times \frac{\partial \vec{B}(\vec{r}')}{\partial t}\right]\mathrm{dV}' \\
&\overset{\nabla \times \vec{B}(\vec{r}')=0}{=} -\frac{1}{4\pi}\int_{\mathrm{V}'} \left[\left(\nabla \frac{1}{|\vec{r}-\vec{r}'|}\right) \times \frac{\partial \vec{B}(\vec{r}')}{\partial t}\right]\mathrm{dV}'.
\end{aligned} \tag{6}$$

Considering the upper bound of the Euclidean norm, namely, the magnitude, of the $\vec{E}_2$, in (7) can be derived

$$\begin{aligned}
\left\|\vec{E}_2\right\| &= \left\| -\frac{1}{4\pi}\int_{\mathrm{V}'} \left[\left(\nabla \frac{1}{|\vec{r}-\vec{r}'|}\right) \times \frac{\partial \vec{B}(\vec{r}')}{\partial t}\right]\mathrm{dV}' \right\| \\
&\le \frac{1}{4\pi}\int_{\mathrm{V}'} \left\| \left(\nabla \frac{1}{|\vec{r}-\vec{r}'|}\right) \times \frac{\partial \vec{B}(\vec{r}')}{\partial t} \right\| \mathrm{dV}' \\
&\le \frac{1}{4\pi}\left\| \frac{\partial \vec{B}(\vec{r}')}{\partial t} \right\|_{\sup} \cdot \int_{\mathrm{V}'} \left\| \frac{\vec{r}'-\vec{r}}{|\vec{r}-\vec{r}'|^3} \right\| \mathrm{dV}' \\
&\le \delta \left\| \frac{\partial \vec{B}(\vec{r}')}{\partial t} \right\|_{\sup}.
\end{aligned} \tag{7}$$

The constant δ in (7) is equal to the largest geometric dimension of V'. Generally, the frequency of the current of the high-voltage transmission line is relatively low and its amplitude is not high. As a result, the derivative of its magnetic field with respect to time is relatively small, implying that the value of $\|\frac{\partial \vec{B}(\vec{r}')}{\partial t}\|_{\sup}$ is very small. It follows that the amplitude of the solenoidal field is extremely small compared with the Coulomb E-field. Therefore, the E-field of general high-voltage equipment except air-core reactor is an electric quasi-static field.

B. Proof of the Linear Relationship Between the Electric Quasi-Static Field and the Voltage

A general multiconductor system made up of *n* conductors and the ground is considered to explain the linear correspondence between the quasi-static E-field and the voltage, as exhibited in Fig. 6. Its static E-field can be expressed as the negative gradient of the electric potential function: $\vec{E} = -\nabla\varphi(\vec{r})$. The potential function at points in the air obeys the Laplace's Equation: $\nabla^2\varphi = 0$. The boundary conditions should be determined to solve the Laplace's equation. The potential of the ground is set to be zero, and the potential of the *i*th conductor is denoted as V_i.

The multiconductor system can be treated as a capacitance network, and the capacitors connected to the *i*th conductor are presented in Fig. 6. Thus, the charge on the conductor is a linear

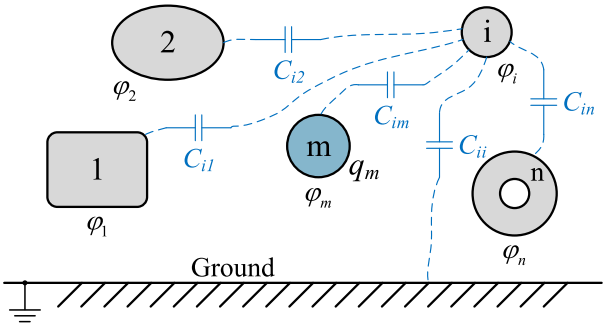

Fig. 6. General multiconductor system.

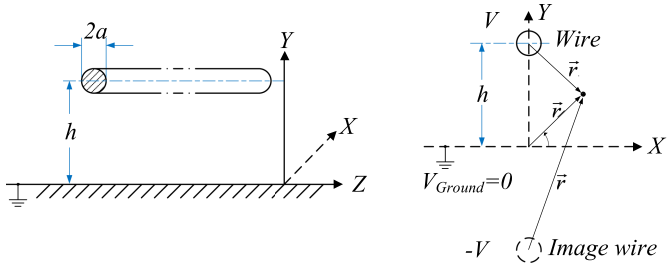

Fig. 7. Single-conductor transmission line (left) and its schematic diagram when using the image method (right).

combination of the conductor potentials [16], as expressed in

$$\begin{pmatrix} q_1 \\ \vdots \\ q_i \\ \vdots \\ q_n \end{pmatrix} = \begin{pmatrix} c_{11} & c_{12} & \cdots & c_{1n} \\ c_{21} & c_{22} & \cdots & c_{2n} \\ \vdots & \vdots & \cdots & \vdots \\ c_{n1} & c_{n2} & \cdots & c_{nn} \end{pmatrix} \begin{pmatrix} V_1 \\ \vdots \\ V_i \\ \vdots \\ V_n \end{pmatrix} \tag{8}$$

where $[c]$ denotes the matrix of capacitance coefficients. $[c]$ represents a physical property of the multiconductor system, which depends on the geometry of the conductors and the permittivity of the medium between the conductors. Equation (9) can be derived as

$$\begin{pmatrix} V_1 \\ \vdots \\ V_i \\ \vdots \\ V_n \end{pmatrix} = \begin{pmatrix} p_{11} & p_{12} & \cdots & p_{1n} \\ p_{21} & p_{22} & \cdots & p_{2n} \\ \vdots & \vdots & \cdots & \vdots \\ p_{n1} & p_{n2} & \cdots & p_{nn} \end{pmatrix} \begin{pmatrix} q_1 \\ \vdots \\ q_i \\ \vdots \\ q_n \end{pmatrix} \tag{9}$$

where $[p]$ indicates the matrix of electric potential coefficients. Thus, the Dirichlet boundary conditions can be determined if the net charge on each conductor is known.

Assume that the quantity of the electric charge on the mth conductor is q_m and other conductors are not charged. Then, the potential of each conductor can be determined, as indicated in (10). Assume that $\psi(\vec{r})$ is the solution to this boundary value problem. In this way, the E-field is $\vec{E}_{q_m} = -\nabla\psi(\vec{r})$

$$q_i = \begin{cases} q_m & i = m \\ 0 & i \neq m \end{cases} \xrightarrow{(9)} \begin{cases} V_i = p_{im} q_m \ i = 1, \cdots, n \\ V_{\text{Ground}} = 0 \end{cases}. \tag{10}$$

Obviously, increasing the net charge on the mth conductor by a factor of α would increases the potentials on all conductors by the same factor of α, as shown in

$$q_i = \begin{cases} \alpha q_m & i = m \\ 0 & i \neq m \end{cases} \xrightarrow{(9)} \begin{cases} V_i = \alpha p_{im} q_m \ i = 1, \cdots, n \\ V_{\text{Ground}} = 0 \end{cases}. \tag{11}$$

At this point, the solution of the Dirichlet boundary value problem becomes $\alpha\psi(\vec{r})$, and the E-field becomes $\vec{E}_{\alpha q_m} = -\alpha\nabla\psi(\vec{r})$, according to the uniqueness theorem. Therefore, the E-field is directly proportional to the potential of the mth conductor, namely, the voltage of the mth conductor

$$\vec{E}_{q_m} \propto V_m. \tag{12}$$

If the conductors are all charged, the total E-field will be the superposition of the E-fields generated by each conductor: $\vec{E} = \sum_{i=1}^{n} \vec{E}_{q_i}$. Therefore, the magnitude of the vertical E-field is the linear combination of the voltages of each conductor

$$E_\perp = \sum_{i=1}^{n} \left|\vec{E}_i\right| \cdot \cos\theta_i = \sum_{i=1}^{n} \beta_i \cdot V_i. \tag{13}$$

Furthermore, the voltages of the conductors $[V_i]$ can be calculated from the measured vertical E-fields [see (13)]. The coefficient matrix $[k]$ can be obtained by calibration

$$\begin{pmatrix} V_1 \\ \vdots \\ V_i \\ \vdots \\ V_n \end{pmatrix} = \begin{pmatrix} k_{11} & k_{12} & \cdots & k_{1n} \\ k_{21} & k_{22} & \cdots & k_{2n} \\ \vdots & \vdots & \cdots & \vdots \\ k_{n1} & k_{n2} & \cdots & k_{nn} \end{pmatrix} \begin{pmatrix} E_1 \\ \vdots \\ E_i \\ \vdots \\ E_n \end{pmatrix}. \tag{14}$$

C. Example: Single-Conductor Transmission Line

The linear correspondence between the E-field and the voltage is illustrated with the single-conductor transmission line as an example. A single wire of infinite length is parallel to the ground plane, as exhibited in Fig. 7. The radius of the wire is a, and the height of the wire is h, $h \gg a$.

Considering the E-field at point $\vec{r}$ on the cross section of the transmission line, the expression of the E-field at the point $\vec{r}$ is given in (15) using the image method

$$\vec{E}(\vec{r}) = \frac{V}{\left(\ln\frac{2h-a}{a}\right)\left|\vec{r}_+\right|^2}\vec{r}_+ - \frac{V}{\left(\ln\frac{2h-a}{a}\right)\left|\vec{r}_-\right|^2}\vec{r}_-. \tag{15}$$

Obviously, the E-field of the single-conductor transmission line is directly proportional to its voltage: $\vec{E}(\vec{r}) \propto V$. Similarly, it can be verified that the magnetic field of the single-conductor transmission line is directly proportional to its current: $\vec{H}(\vec{r}) \propto I$. Thus, the active and reactive power transmitted by the single-conductor transmission line will be determined by its electric and magnetic fields.

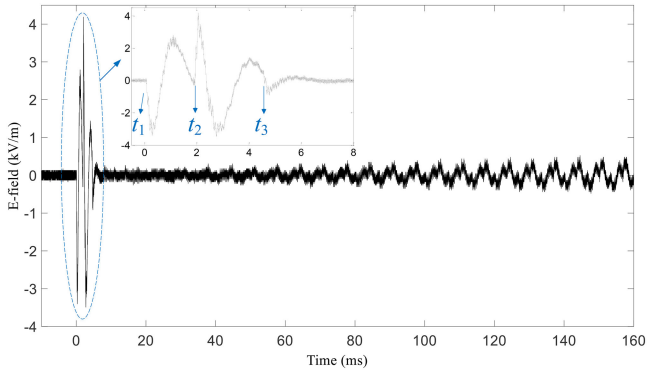

Fig. 8. Transient E-field waveform at measuring point 4 during the MMC startup.

IV. Switching E-field Pulses of the MMC and HVDC CB and Its Application in Improving the Measurement Accuracy of Action Moment

A. Measurement of the Closing Time Intervals Between Three Phases During the Closing Operation of the AC CB When MMC is Started

At the beginning of the test, the capacitors of the MMC are not charged, and the converter station is not connected to the dc grid. Thus, the MMC is charged from the ac grid. There are voltage and current surges when the ac CB in Hall 1 is closed, leading to strong transient EMI. The current limiting resistors can suppress the surges and EMI to a certain extent but cannot eliminate them.

Fig. 8 displays the transient E-field waveform at measuring point 4 when the ac CB is closed. The two dc CBs remain closed during the MMC startup, and the measurement result is the E-field below the negative dc bus. Owing to the voltage phase difference and the mechanical structure difference between the three phases of the ac CB, the three phases of the CB cannot be closed at the same time. The closing time intervals between the three phases measured by the waveform recording system that comes with the converter station are about 2 ms. More accurate time intervals can be obtained with the E-field pulse measurement. As can be seen from the zoomed-in waveform in Fig. 8, the closure of each phase excites a pulse with a steep pulse front edge. Hence, the first, second, and third phases are closed at $t_1 = 0$ ms, $t_2 = 1.854$ ms, and $t_3 = 4.489$ ms, respectively, with an measurement error of less than 0.005 ms.

B. Measurement of the Action Moment of the MMC by the Switching E-field Pulses

1) MMC Operating Information Leaked by the High-Frequency E-field: The equivalent circuit diagram of the MMC when it is blocked is illustrated in Fig. 9. U_a, U_b, and U_c are the three-phase ac voltages of the MMC. U_+ and U_- indicate the voltages of the positive and negative busbars. C_0 and C_{eq} represent the equivalent capacitance of each bridge arm and the stray capacitance between the busbar and the ground, respectively.

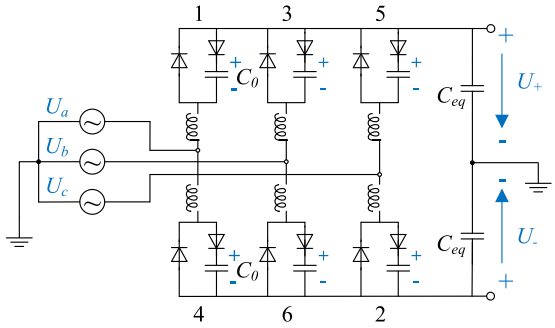

Fig. 9. Equivalent circuit diagram of the MMC when it is blocked.

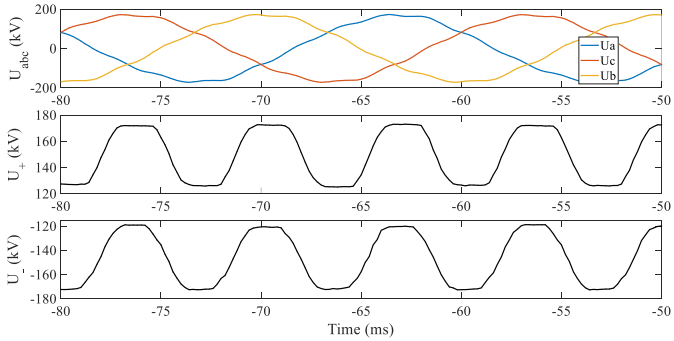

Fig. 10. Ac-side and dc-side voltage waveforms of the MMC.

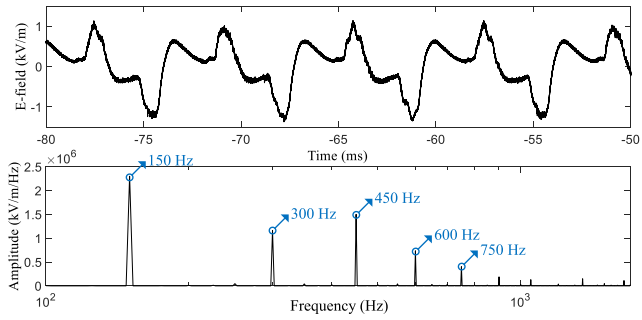

Fig. 11. E-field waveform and spectrum measured at measuring point 3 when the MMC is blocked.

Fig 10 exhibits the ac-side and dc-side voltage waveforms of the MMC measured by the waveform recording system that comes with the converter station. The U_+ and U_- fluctuate with the three-phase ac voltages. Fig. 11 presents the synchronous E-field measured at the measuring point 3. Spectrum analysis suggests that the fundamental frequency of the E-field wave is 150 Hz, and it also includes second, third, fourth, fifth, and other harmonics. However, the higher frequency harmonics of U_+ and U_- is not as significant as in the E-field waveform. This is in that the measurement bandwidth of the waveform recording system that comes with the converter station is limited, and the high-frequency components of the voltage are attenuated. Consequently, the measured E-field can provide information on the high-frequency harmonics, which are filtered out by the voltage measurement system built in the converter station.

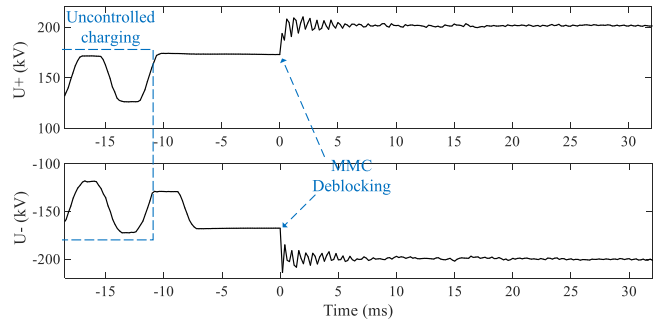

Fig. 12. Voltage waveform of the positive and negative busbars during deblocking of the MMC.

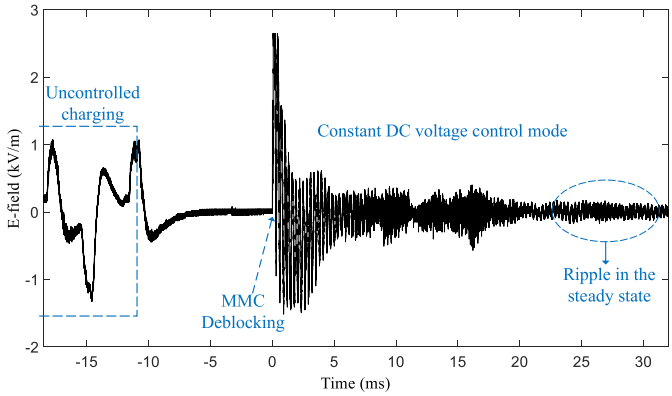

Fig. 13. E-field waveform measured at measuring point 3 during operating mode switching of the MMC.

The voltage waveforms of the positive and negative busbars during deblocking of the MMC are displayed in Fig. 12. Since the voltage of the dc bus can only reach about 70% of the rated voltage in the uncontrollable charging mode, a severe voltage surge occurs when the valves are deblocked, resulting in an instantaneous E-field pulse, as shown in Fig. 13. Thus, the moment of the MMC deblocking can be accurately determined by the steep rising edge of this E-field pulse. In the steady-state after startup, the MMC adopts the NLM control strategy, and the high-speed switching operation of the submodules will generate high-frequency ripples on the E-field waveform.

2) Accurate Measurement of the MMC Emergency Blocking Action Moment in the Single-Pole-to-Ground Short-Circuit Test: In the single-pole-to-ground short-circuit test, the voltage waveforms and the action moments, t_0 to t_4, of the MMC and CB are illustrated in Fig. 14. At $t_0 = 0$ ms, the positive bus is artificially grounded, and its voltage drops to zero. Immediately, the voltage of the negative bus doubles, and the MOA of the negative is broken down. Thus, the negative voltage is clamped to the residual voltage of the MOA. The equivalent circuit of the MMC and dc CB when the single-pole-to-ground short-circuit occurs is illustrated in Fig. 15. The elements through which the short-circuit current flows are drawn with red lines.

After the set time has elapsed, the MMC is emergently blocked at t_1. The equivalent circuit when the MMC is blocked is shown

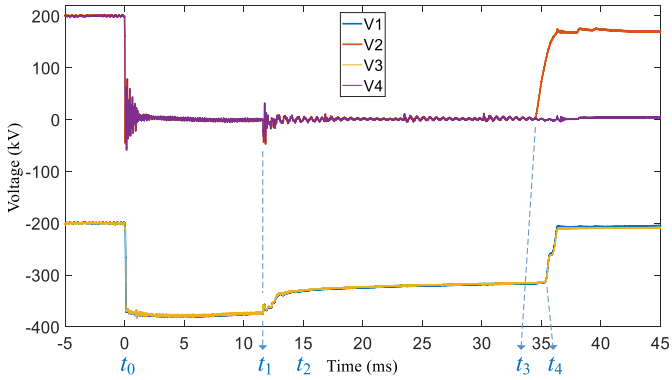

Fig. 14. Voltage waveforms during the single-pole-to-ground short-circuit test.

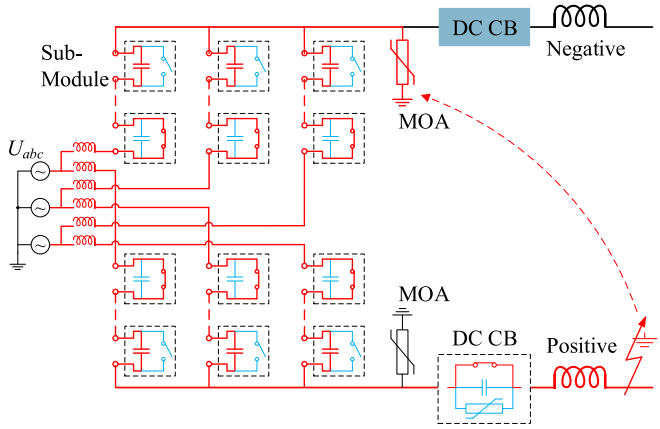

Fig. 15. Equivalent circuit of the MMC and dc CB from t_0 to t_1.

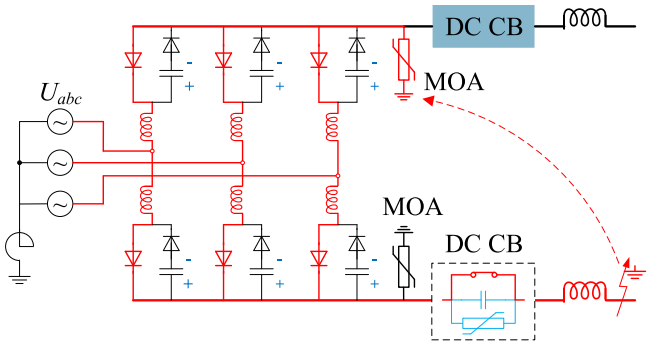

Fig. 16. Equivalent circuit of the MMC and dc CB from t_1 to t_3.

in Fig. 16. At this time, the short-circuit current is maintained by the freewheel diode.

The HVdc CB should break to cut off the short-circuit current completely to protect the valve. The main current branch is blocked at $t_2 \approx 15$ms. However, the blocking of the main current branch does not affect the voltage waveforms. Next, the blocking of the current commutation branch insert the MOV of the dc CB into the current loop, and the voltage on the positive wire rises from time t_3. The equivalent circuit of the MMC and the dc CB after the blocking of the current commutation branch is provided in Fig. 17. Under the effect of the continuous currents of

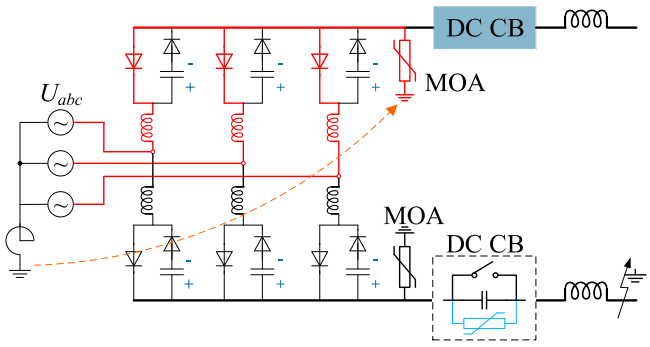

Fig. 17. Equivalent circuit of the MMC and dc CB from t_3 to t_4.

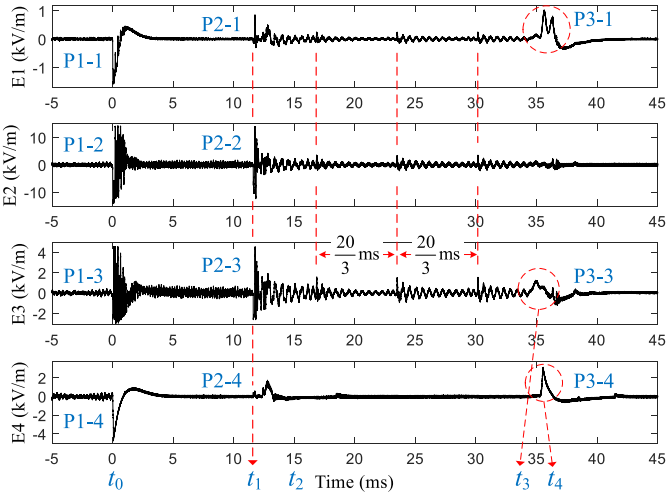

Fig. 18. E-field pulses during the single-pole-to-ground short-circuit test.

the inductors, the negative MOA recovers at t_4, approximately 1 ms after t_3, leading to a voltage step on the negative wire. Since the short-circuit current is not very large, the MOV of the HVdc CB does not act. Therefore, part of the energy stored in the inductors is dissipated by the MOA, and the other part is stored in the capacitors of the current commutation branch of the positive HVdc CB.

The measured E-field pulses during the single-pole-to-ground short-circuit test are shown in Fig. 18. As revealed by comparing with the voltage waveforms, the E-field pulses correspond to the sudden changes in the voltage. The first pulse P1 is induced by the short-circuit. Pulses P1-2 and P1-3 indicate that the transient E-field below the grounded positive bus has strong oscillations. The emergency blocking of the MMC generates the E-field pulse P2, which is zoomed-in in Fig. 19. Through the steep front of the pulses, the blocking moment of the MMC is determined as $t_1 =$ 11.607 ms with an error of less than 0.005 ms. The subsequent periodic pulses with a period of 20/3 ms reflect that the blocked MMC dischargs through the short-circuit point. Blocking the main current branch of the CB at t_2 has no effect on the E-field waveform. Nonetheless, the current commutation between Branch 1 and Branch 2 in Fig. 4 can induce transient magnetic pulse. The voltage change of the positive wire at t_3 is relatively

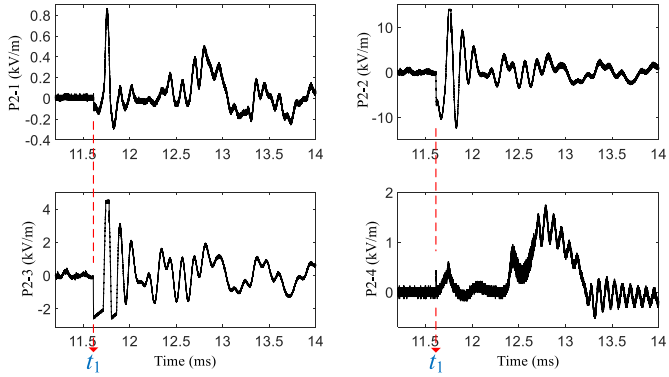

Fig. 19. E-field pulses generated by the emergency blocking of the MMC.

TABLE I
TIME SEQUENCE OF THE RELAY PROTECTION ACTION OF THE MMC AND THE HVDC CB IN THE SINGLE-POLE-TO-GROUND SHORT-CIRCUIT TEST

Time	Relay protection action	E-pulse
t_0= 0 ms	Positive wire shorted to the ground	P1
t_1= 11.607 ms	Emergency blocking of the MMC	P2
$t_2 \approx$ 15 ms	Blocking of the main current branch of the CB	None
$t_3 \approx$ 34.5 ms	Blocking of the current commutation branch of the CB	P3-3
$t_4 \approx$ 35.4 ms	Recovery of the negative MOA	P3-1, P3-4

slow, so only a slow pulse P3-3, is detected below the busbar between the positive CB and the MMC. The pulses P3-1 and P3-4 are measured next to the negative busbar. They are generated by the voltage rise of the negative busbar caused by the recovery of the MOA.

The abovementioned analysis demonstrates that the measured E-field below the busbar corresponds to the high-frequency component of the voltage. Differences in the voltage waveforms on different busbar segments lead to significant differences in the E-field waveforms at different measuring points. The corresponding relationship between the relay protection actions and the E-field pulses is summarized in Table I. Among them, the action moment of the short-circuit and the MMC emergency blocking can be accurately measured by the sharp E-field pulse, and the error can be less than 0.005 ms.

C. Measurement of the Blocking Action Moment of the Current Commutation Branch of the HVDC CB in the Short-Circuit Test Between the Positive and Negative Cables

As Fig. 20 shows, the positive and negative cables are shorted together at $t_0 = 0$ ms, and the voltage on the positive and negative buses drops rapidly. Concurrently, the resonance between the smoothing reactor and the equivalent capacitor of the MMC enables the voltage waveform to oscillate strongly. The equivalent circuit of the MMC and dc CB when the pole-to-pole short-circuit occurs is shown in Fig. 21.

The large short-circuit current triggers the emergency blocking of the MMC and the breaking operation of the CB. The main current branch of the CB is blocked at $t_1 \approx$ 1ms, and the voltage waveforms are not affected by this. The MMC is blocked at t_2,

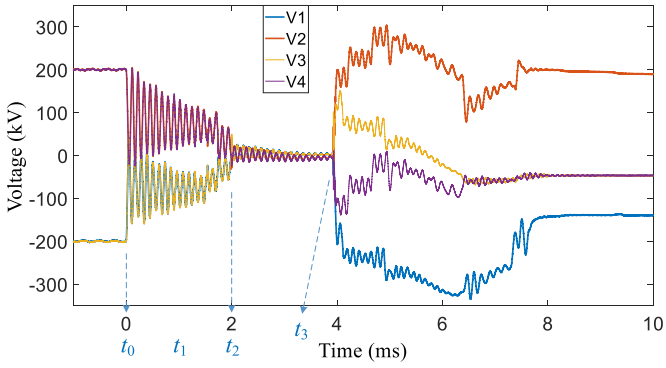

Fig. 20. Voltage waveforms during the short-circuit test between the positive and negative cables.

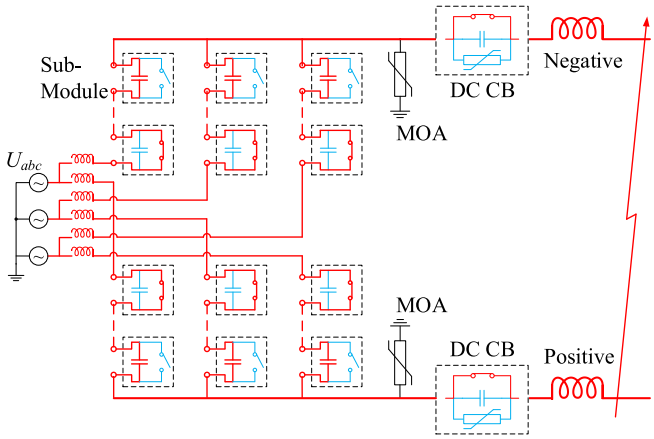

Fig. 21. Equivalent circuit of the MMC and dc CB from t_0 to t_2.

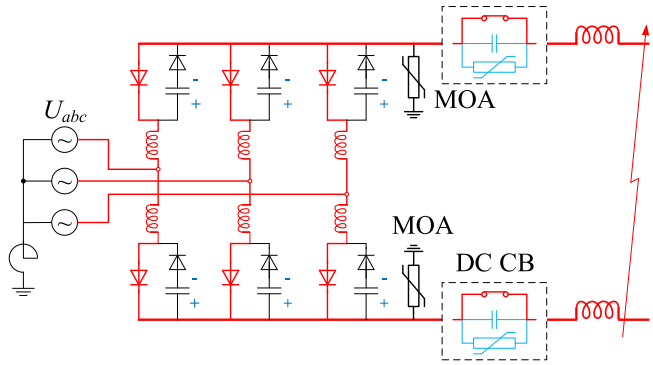

Fig. 22. Equivalent circuit of the MMC and dc CB from t_2 to t_3.

causing a sudden voltage sag. The equivalent circuit when the MMC is blocked is shown in Fig. 22.

The blocking of the current commutation branch at t_3 breaks the short-circuit current and produces a fast step and oscillation in the voltage waveforms. The equivalent circuit when the dc CBs are open is shown in Fig. 23. The voltage waveform in Fig. 20 changes much faster at t_3 compared to the voltage in Fig. 14. This is because the short-circuit current between the positive and the negative cables is much larger than the short-circuit current between the positive cable and the ground. Consequently,

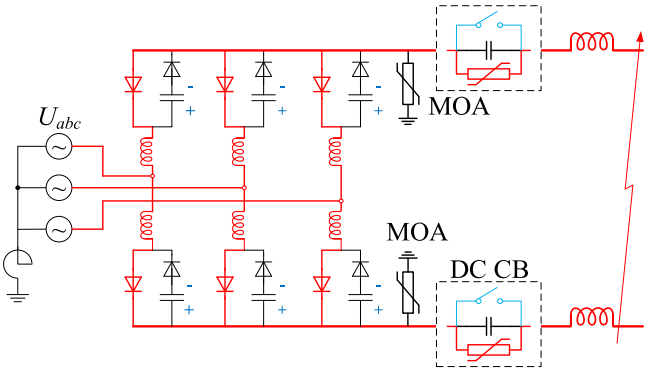

Fig. 23. Equivalent circuit of the MMC and dc CB after t_3.

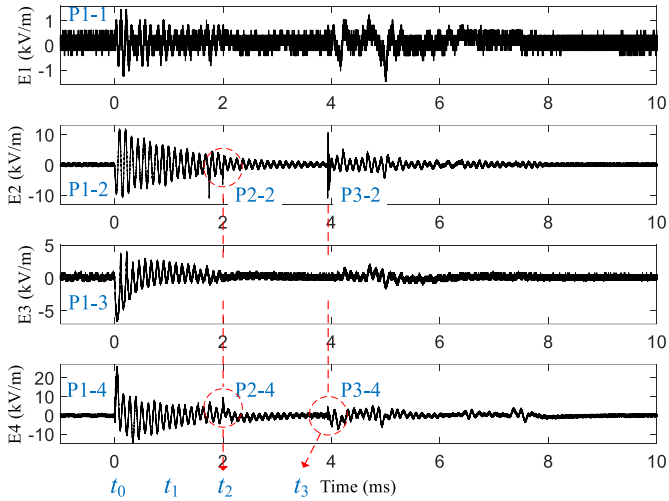

Fig. 24. E-field pulses during the short-circuit test between the positive and negative cables.

the voltage across the capacitors in the current commutation branch of the CB increases much faster and oscillates with the system inductance. Then, the stored energy in the system inductance is dissipated by the MOV of the CB. Owing to the nonlinear characteristic of the MOV, the voltage fluctuates and oscillates after time t_3.

The measured E-field pulses during the short-circuit test between the positive and the negative cables are presented in Fig. 24 . The first pulse P1, caused by the short-circuit, has strong oscillation, and its dominant frequency is consistent with the dominant frequency of the voltage oscillation. Blocking the main current branch of the CB at t_1 does not affect the E-field waveform, in line with the effect on the voltage. The blocking of the MMC at t_2 and the blocking of the current commutation branch of the CB at t_3 generate P2 and P3, respectively. The pulses P3-2 and P3-4 in Fig. 24 are much faster than the pulse P3-3 in Fig. 18, in good agreement with the voltage variation.

There are significant differences between the four transient E-field waveforms. The E-field waveform E1 is measured at the midpoint of the two CBs. The E-field at this point is expected to have a large horizontal component and a small vertical component. As expected, the measurement results demonstrate

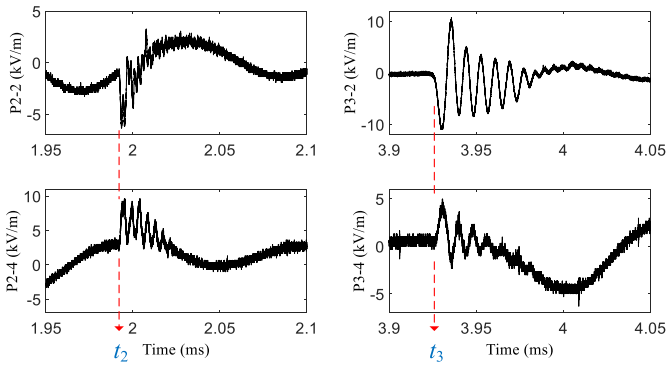

Fig. 25. Zoomed-in waveforms of P2-2, P2-4, P3-2, and P3-4 in Fig. 24.

TABLE II
TIME SEQUENCE OF THE RELAY PROTECTION ACTION OF THE MMC AND THE HVDC CB IN THE SHORT-CIRCUIT TEST BETWEEN THE POSITIVE AND NEGATIVE CABLES

Time	Relay protection action	E-pulse
t_0= 0 ms	The positive wire shorted to the negative wire	P1
$t_1 \approx 1$ ms	Blocking of the main current branch of the CB	None
t_2= 1.992 ms	Emergency blocking of the MMC	P2-2, P2-3
t_3= 3.925 ms	Blocking of the current commutation branch of the CB	P2-4, P3-4

TABLE III
ACTION MOMENT THAT CAN BE MEASURED BY THE SWITCHING E-FIELD PULSE IN THIS TEST

Power equipment	Action moment
Dc cable	The moment when the short circuit fault occurs
Ac CB	Closing operation Closing time intervals between the three phases
MMC	Deblocking Emergency blocking
HVdc CB	Blocking of the current commutation branch Blocking moment of the main current branch can be determined by the magnetic field pulse

that the amplitude of E1 is the smallest of the four vertical E-field waveforms. The E-field waveforms E2, E3, and E4 correspond to the high-frequency components of the voltages of the adjacent busbars or their linear combination, implying significant differences between them.

The E-field waveform should be smooth. In other words, its derivative should be continuous. The reason is that the magnetic field generated by the displacement current $\varepsilon_0 \cdot \partial \vec{E}/\partial t$ should be continuous. On the other hand, the measurement noise is inevitable. Hence, only an interval containing the true value of the action moment can be determined based on the steep pulse front of the switching E-field pulse. The zoomed-in waveforms of P2-2, P2-4, P3-2, and P3-4 are shown in Fig. 14. The action moments t_2 and t_3 determined by these waveforms are listed in Table II. Following the steep pulse fronts of these pulses, the error in the measured action moment can be less than 0.005 ms.

V. CONCLUSION AND SUGGESTIONS

The use of electromagnetic fields to transfer energy has a long history. Two of the most basic physical quantities of the power system are voltage and current. Essentially, voltage is the integral of the electric field and current is the integral of the magnetic field. In this article, the linear correspondence between the E-field of the high voltage equipment and its voltage has been verified by theoretical analysis and measurement experiments. Spectral analysis reveals that the switching E-field pulses measured in the Zhouding converter station are majorly distributed below 300 kHz. Considering the size of the power equipment in the converter station, the measured transient E-field below the busbar next to the HVdc CB is an electric quasi-static field. Therefore, the measured switching E-field pulse should be proportional to the high-frequency components of the voltages of the adjacent busbars or their linear superposition.

Based on this principle, a switching E-field pulse-based MMC and HVdc CB action moment measurement method is proposed. This method is noninvasive, flexible and of low cost. To a certain extent, it can make up for the shortcoming of the fault recording system that comes with the converter station. For example, it is found that the high-frequency harmonics, which may be ignored by the voltage recording system built in the converter station, can be detected through the E-field of the power line. The action moments that can be measured in the short-circuit test by this method are listed in Table III. Based on the steep pulse front of the switching E-field pulse, the error in the measured action moment can be less than 0.005 ms.

Since the E-field measurement system in this article cannot measure the signals below 200 Hz, the measured E-field needs to be analyzed in conjunction with the voltage signal. Next, the information fusion method of the high-frequency E-field signal and the low-frequency voltage signal will be studied for the condition monitoring of the converter station. In addition to increasing the measurement bandwidth, the number and location of the measuring points also need to be optimized.

ACKNOWLEDGMENT

The authors would like to thank K.-j. Li from Hefei University of Technology, H. Shen from North China Electric Power University, and C.-y. Liu from Dalian Maritime University for their useful suggestion and discussion.

REFERENCES

[1] G. R. Liu, F. Xu, Z. Xu, Z. R. Zhang, and G. Tang, "Assembly HVDC breaker for HVDC grids with modular multilevel converters," *IEEE Trans. Power Electron.*, vol. 32, no. 2, pp. 931–941, Feb. 2017.

[2] G. S. Liang and R. M. Zhu, "Predictive analysis for radiated electromagnetic disturbance in MMC-HVDC valve hall," *CPSS Trans. Power Electron. Appl.*, vol. 5, no. 2, Jun. 2020.

[3] C. M. Wiggins, D. E. Thomas, F. S. Nickel, and S. E. Wright, "Transient electromagnetic interference in substations," *IEEE Trans. Power Del.*, vol. 9, no. 4, pp. 1869–1884, Sep. 1994.

[4] J. Zhang, T. B. Lu, W. D. Zhang, H. Shen, and Z. C. Yang, "Frequency-time domain characteristics of radiated electric fields in a multi-terminal MMC-HVDC station," *IEEE Access*, vol. 7, pp. 99937–99944, Jul. 2019.

[5] J. Zhang, T. B. Lu, W. D. Zhang, X. M. Bian, and X. Cui, "Characteristics and influence factors of radiated disturbance induced by IGBT switching," *IEEE Trans. Power Electron.*, vol. 34, no. 12, pp. 11833–11842, Dec. 2019.
[6] P. J. Moore, "Radiometric measurement of circuit breaker interpole switching times," *IEEE Trans. Power Del.*, vol. 19, no. 3, pp. 987–992, Jul. 2004.
[7] S. D. Meier, P. J. Moore, and P. F. Coventry, "Radiometric timing of high-voltage circuit-breaker opening operations," *IEEE Trans. Power Del.*, vol. 26, no. 3, pp. 1411–1417, Jul. 2011.
[8] J. L. Roldan, D. Birtwhistle, M. Blundell, and T. Tang, "A noninvasive method for detecting restriking: Application to the switching of HV shunt reactors," *IEEE Trans. Power Del.*, vol. 27, no. 2, pp. 541–547, Apr. 2012.
[9] M. A. Chapman, "Possibilities and limitations of radio-frequency measurement of arc duration in HVAC circiut breakers," Ph.D. dissertation, Dep. of Inform. Technol. Electrical Eng., ETH Zurich, Zurich, Switzerland, 2011.
[10] D. K. Mishra, B. Sarkar, C. Koley, and N. K. Roy, "An unsupervised gaussian mixer model for detection and localization of partial discharge sources using RF sensors," *IEEE Trans. Dielectrics Elect. Insul.*, vol. 24, no. 4, pp. 2589–2598, Aug. 2017.
[11] X. Kong *et al.*, "High-voltage circuit breaker insulation fault diagnosis in synthetic test based on noninvasive switching electric field pulses measurement," *IEEE Trans. Power Del.*, vol. 31, no. 3, pp. 1168–1175, Jul. 2016.
[12] N. A. Belda and R. P. P. Smeets, "Test circuits for HVDC circuit breakers," *IEEE Trans. Power Del.*, vol. 32, no. 1, pp. 285–293, Feb. 2017.
[13] S. L. Jia, Q. Tang, and Z. Q. Shi, "Review on HVDC circuit-breaker tests," in *Proc. 4th Int. Conf. HVDC*, 2020, pp. 808–814.
[14] X. Kong, W. Q. Xing, Y. Z. Xie, Z. Zheng, and Z. D. Sun, "A broadband optical fiber transmission-based time-domain measurement system for nanosecond-level transient electric field," *Rev. Sci. Instruments*, vol. 93, no. 1, Jan. 2022.
[15] D. K. Cheng, "Chapter II: Vector analysis," in *Field and Wave Electromagnetics*, 2nd ed., D. Cheng, Ed. New York, NY, USA: Pearson Education, 1989, pp. 63–66.
[16] W. R. Smythe, "Chapter II: Capacitors, dielectrics, system of conductors," in *Static and Dynamic Electricity*, 3rd ed., W. R. Smythe, Ed. New York, NY, USA: Taylor & Francis, 1989, pp. 28–38.

Xu Kong was born in Shandong, China, in 1988. He received the Ph.D degree in electrical engineering from Xi'an Jiao Tong University, Xi'an, China, in Jun. 2018.

He is currently a Lecturer with the College of Electrical Engineering and Automation, Shandong University of Science and Technology. His research interest includes transient electromagnetic field measurement.

Yan-zhao Xie (Senior Member, IEEE) was born in Henan, China, in 1973. He received the Ph.D. degree in electrical engineering from Tsinghua University, Beijing, China.

He is currently a Full Professor with the School of Electrical Engineering, Xi'an Jiaotong University, Xi'an, China. His research interests include transient analysis of multiconductor transmission lines, electromagnetic transients in power systems, and high power electromagnetics, etc.

Dr. Xie has been a Member of National Standardization Committee of high power transients and a Member of Academic Committee of a State-Level Key Laboratory in China.

Wen-qi Xing was born in Hebei, China, in 1987. He received the master's degree in electrical engineering from Xi'an Jiaotong University, Xi'an, China.

He is currently an Engineer in the Pinggao Group Co., Ltd., Pingdingshan, China.

Zhen-dong Sun (Senior Member, IEEE) received the B.S. degree in applied mathematics with the Ocean University of China, Qingdao, China, in 1990, the M.S. degree in cybernetics and operational research at Xiamen University, Xiamen, China, in 1993, and the Ph.D. degree from the Beijing University of Aeronautics and Astronautics, Beijing, China, in 1996.

He was a Postdoctoral Research Fellow with Tsinghua University, Beijing, China; Associate Professor with the Beijing University of Aeronautics and Astronautics; Senior Research Fellow with the National University of Ireland, Maynooth, Ireland; Professor with the South China University of Technology, Guangzhou, China; and Researcher with the the Academy of Mathematics and Systems Science, Chinese Academy of Sciences, Beijing, China. He is currently with the College of Electrical Engineering and Automation, Shandong University of Science and Technology, Qingdao, China, as a Professor. He is author of two monographs on switched systems. His current research interests include switched and hybrid systems.

Dr. Sun was an Associate Editor for the IEEE TRANSACTIONS ON AUTOMATIC CONTROL and Subject Editor of the *International Journal of Robust & Nonlinear Control.*

Shao-yin He (Member, IEEE) received the Ph.D. degree in electrical engineering from Xi'an Jiaotong University, Xi'an, Shaanxi, China, in June 2019.

His research interests include electromagnetic transients, power system protection, and time reversal technique.

Peng Qiu received the M.S. degree from Zhejiang University, Hangzhou, China, in 2011. He is currently a Senior Engineer with the State Grid Zhejiang Electric Power Company.

Xiao-jun Ni was born in Zhejiang, China, in 1989. He received the Ph.D. degree from North China Electric Power University (NCEPU), Beijing, China.

He is currently an engineer in State Grid Zhejiang Electric Power Co., Ltd Research Institute.

Li Liu received the M.S. degree from the Huazhong University of Science and Technology, Wuhan, China, in 2011.

She is currently a Senior Engineer in the State Grid Zhejiang Electric Power Company.

Kun Zhang was born in Henan, China, in 1985. He received the B.S. degree in electrical engineering from Wuhan University, Wuhan, China.

He is currently with XJ Electric Co., Ltd., Xuchang, China.